AGU PUBLICATIONS

JGR

Journal of Geophysical Research: Biogeosciences

RESEARCH ARTICLE
10.1002/2017JG003877

Key Points:
- Tree island soil CO_2 concentrations were as high as 200,000 ppm (0.30 m depth)
- Mean 2015 soil CO_2 efflux at the site was 0.023 ± 0.103 mg CO_2-C m^{-2} s^{-1}
- The gradient method presents challenges for application in the Pantanal

Supporting Information:
- Supporting Information S1

Correspondence to:
M. J. Lathuillière,
mlathuilliere@alumni.ubc.ca

Citation:
Lathuillière, M. J., O. B. Pinto Jr., M. S. Johnson, R. S. Jassal, H. J. Dalmagro, N. K. Leite, A. B. Speratti, D. Krampe, and E. G. Couto (2017), Soil CO_2 concentrations and efflux dynamics of a tree island in the Pantanal wetland, *J. Geophys. Res. Biogeosci.*, *122*, doi:10.1002/2017JG003877.

Received 6 APR 2017
Accepted 8 AUG 2017
Accepted article online 14 AUG 2017

Soil CO_2 concentrations and efflux dynamics of a tree island in the Pantanal wetland

Michael J. Lathuillière[1], Osvaldo B. Pinto Jr[2], Mark S. Johnson[1,3], Rachhpal S. Jassal[4], Higo J. Dalmagro[2], Nei K. Leite[5], Alicia B. Speratti[1], Daniela Krampe[6], and Eduardo G. Couto[7]

[1]Institute for Resources, Environment and Sustainability, University of British Columbia, Vancouver, British Columbia, Canada, [2]Programa de Pós-Graduação em Ciências Ambientais, Universidade de Cuiabá, Cuiabá, Brazil, [3]Department of Earth, Ocean and Atmospheric Sciences, University of British Columbia, Vancouver, British Columbia, Canada, [4]Faculty of Land and Food Systems, University of British Columbia, Vancouver, British Columbia, Canada, [5]Centro de Ciências Biológicas, Universidade Federal de Santa Catarina, Florianópolis, Brazil, [6]Faculty of Geography, Philipps-University Marburg, Marburg, Germany, [7]Departamento de Solos e Engenharia Rural, Universidade Federal de Mato Grosso, Cuiabá, Brazil

Abstract The Pantanal is the largest tropical wetland on the planet, and yet little information is available on the biome's carbon cycle. We used an automatic station to measure soil CO_2 concentrations and oxidation-reduction potential over the 2014 and 2015 flood cycles of a tree island in the Pantanal that is immune to inundation during the wetland's annual flooding. The soil CO_2 concentration profile was then used to estimate soil CO_2 efflux over the two periods. In 2014, subsurface soil saturation at 0.30 m depth created conditions in that layer that led to CO_2 buildup close to 200,000 ppm and soil oxidation-reduction potential below −300 mV, conditions that were not repeated in 2015 due to annual variability in soil saturation at the site. Mean CO_2 efflux over the 2015 flood cycle was 0.023 ± 0.103 mg CO_2-C m^{-2} s^{-1} representing a total annual efflux of 593 ± 2690 mg CO_2-C m^{-2} y^{-1}. Unlike a nearby tree island site that experiences full inundation during the wet season, here the soil dried quickly following repeated rain events throughout the year, which led to the release of CO_2 pulses from the soil. This study highlights not only the complexity and heterogeneity in the Pantanal's carbon balance based on differences in topography, flood cycles, and vegetation but also the challenges of applying the gradient method in the Pantanal due to deviations from steady state conditions.

Plain Language Summary The Pantanal is the largest wetland in the world whose carbon balance is expected to change with seasonal flooding, especially in tree islands that can be immune to flooding. We provide a half-hourly time series of soil CO_2 concentrations, efflux, and oxidation-reduction potential at a tree island site in the Pantanal. Soil CO_2 concentration at 0.30 m depth was as high as 200,000 ppm, while our 2015 average soil efflux estimate using the gradient method was 0.023 mg CO_2-C m^{-2} s^{-1}. Our results allow for a spatial assessment of soil CO_2 effluxes in the Pantanal, revealing complex biogeochemical processes in the tropical wetland with controls more heavily influenced by topography and vegetation. This research also highlights instrumental challenges in applying the gradient method in the tropical wetland.

1. Introduction

Wetlands consist of a variety of hydrologic landscapes (e.g., lakes, peats, and marshes), which collectively act as important centers of cultural, economic, and biological diversity [*Mitsch and Gosselink*, 2015] offering key ecosystem services such as flood or climate regulation, groundwater recharge, or water purification [*Millenium Ecosystem Assessment*, 2005]. While wetlands cover 4–6% of the planet's surface [*Mitra et al.*, 2005], this number is rapidly decreasing due to local and global threats from population growth, agricultural expansion, or climate change [*Junk et al.*, 2013]. Wetlands play an important role in regional and global carbon (C) cycles [*Neue et al.*, 1997]. Global wetland soils are estimated to contain 202–535 Pg C in soil organic carbon at densities ranging from 375 to 723 Mg C ha^{-1} depending on wetland definitions [*Mitra et al.*, 2005], but these values may increase or decrease based on wetland management.

Tropical wetlands represent 30% of the world's wetlands, although knowledge remains limited on their biogeochemistry, C sequestration, and methane emissions [*Mitsch et al.*, 2010]. Low decomposition rates in anaerobic soils are believed to be key mechanisms of C sequestration in wetlands worldwide

[*Mitra et al*., 2005]. These rates, however, may change in the tropics due to higher temperatures [*Mitsch and Gosselink*, 2015], thus affecting local and global C balances [*Mitsch et al*., 2010]. Soil C sequestration has been estimated for tropical wetlands in Costa Rica at 250–260 g C m^{-2} y^{-1} [*Mitsch et al*., 2010] with values that are greater than the global range of soil C sequestration reported by *Mitra et al*. [2005] of 20–140 g C m^{-2} y^{-1}.

Carbon cycle studies in tropical wetlands have been of great interest in light of human development and climate change pressures [*Junk et al*., 2013]. Carbon losses from tropical wetlands occur through various pathways including (1) evasion of CO_2 from soil and flood waters, (2) water-air gas exchange through vegetation and respiration, and (3) loss in dissolved organic and inorganic C, including black C from the burning of biomass. Water-air CO_2 exchanges in flood waters have been reported in tropical wetlands such as Australia (750 g C m^{-2} y^{-1}) [*Bass et al*., 2014], the upper Rio Negro basin of Amazonia (800 g C m^{-2} y^{-1}) [*Belger et al*., 2011], and the Pantanal wetland (1288 g C m^{-2} y^{-1}) [*Hamilton et al*., 1995]. Production of CO_2 in soils results from microbial (heterotrophic) and root (autotrophic) respiration and varies in response to soil organic C content as well as soil temperature and water content [*Kim et al*., 2012; *Jassal et al*., 2004]. In wetlands, successive chemical and biological processes take place in the soil following inundation described by a successive drop in oxidation-reduction potential [*Pezeshki and Delaune*, 2012]. Under acidic conditions (e.g., pH $<$ 4.5) sequential electrochemical reductions include denitrification (oxidation-reduction potential E_h = 850 mV), the reduction of Fe^{3+} to Fe^{2+} (E_h = 550 mV), and the reduction of CO_2 into CH_4 (E_h = −100 mV) [*Vepraskas and Faulkner*, 2000]. At the same time, anaerobic conditions in the soil favor CH_4 emissions through methanogenesis from microbial activity. Tropical wetland CH_4 emissions range from 26 to 75 Tg C y^{-1} [*Mitra et al*., 2005].

Data on year-round temporal changes in soil CO_2 concentrations and effluxes in wetlands are limited in the literature, especially in tropical wetlands [*Kim et al*., 2012]. Despite playing an important role in the C budget [*Aufdenkampe et al*., 2011], tropical wetland soils appear to be a very significant source of C emitted to the atmosphere. *Johnson et al*. [2013] used a multiparameter and autonomous measurement station in the Northern Pantanal, reporting annual CO_2 efflux from the wetland soil of 1220 g C m^{-2} y^{-1}. These measurements were accompanied by high-frequency soil E_h observations, which revealed important information on soil conditions under prolonged inundation, which include possible CH_4 emissions [*Dalmagro et al*., 2016; *Messias et al*., 2013]. Similar measurements are required in other Pantanal landscapes to understand the mechanisms of soil CO_2 dynamics in tropical wetlands and their dependency on local hydrology and vegetation. The use of half-hourly measurements has proven to be greatly informative compared to coarse monthly manual measurements for estimating the C budget of landscapes in the Pantanal. Such information can also inform environmental policy within the greater context of Brazilian wetland definition and classification [*Junk et al*., 2014].

The Pantanal wetland occupies 160,000 km^2 (Figure 1) and is characterized as a temporary (e.g., seasonal) wetland with a monomodal flood pulse [*Junk et al*., 2006]. Biogeochemical cycles in the Pantanal are driven by the wetland's annual flood pulse as river systems break their banks to inundate floodplains and saturate soils, thereby affecting primary and secondary productivity [*Junk*, 2013]. Tree islands, locally known as *cordilheiras*, are unique landscape features of the wetland that can experience various levels of flooding and are considered important for habitat in locations where they do not experience full inundation [*Junk et al*., 2006]. Temperature increases and changes in precipitation patterns in South America are expected to impact wetlands, including the Pantanal [*Junk et al*., 2013]. Tree islands experiencing less frequent flooding may become more common in the Pantanal as a result of a decrease in large flood events.

In this study, we provide half-hourly measurements of soil CO_2 concentrations and estimate fluxes at a tree island in the Brazilian Pantanal during the 2014 and 2015 flood cycles using a multiparameter and autonomous measurement station similar to installations described in previous research [*Johnson et al*., 2013; *Messias et al*., 2013] with the objectives to (1) capture intraannual and interannual changes in soil CO_2 dynamics as influenced by precipitation and soil wetting events and (2) link the C and water cycles in the Pantanal by comparing findings at the tree island to those of a nearby site [*Dalmagro et al*., 2016; *Johnson et al*., 2013] with distinct vegetation and flood events.

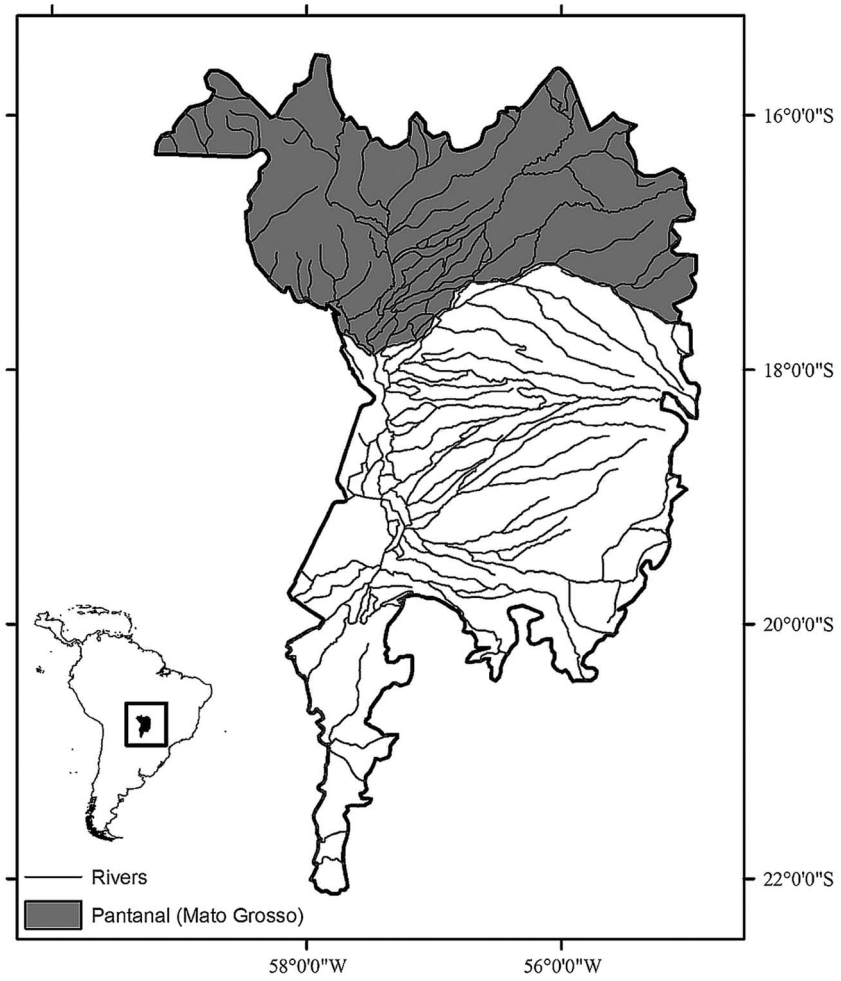

Figure 1. The Pantanal wetland with the Northern region located in Mato Grosso, Brazil.

2. Methods

2.1. Site Description

The tree island site is located in the Northern Pantanal of Mato Grosso, Brazil (16°29′52″S, 56°24′47″W, 120–130 m elevation), on property managed by the Brazilian Social Service of Commerce (SESC) near the municipality of Poconé, about 140 km south of Cuiabá (Figure 2). Micrometeorology measurements made near the site in 2012–2015 recorded annual average temperatures of 24.9°C with annual average minimum and maximum temperatures of 12.5°C and 38.2°C, respectively (see section 2.2). Annual precipitation between 2012 and 2014 was 1596 mm y^{-1} with a pronounced dry season (May to September, 232 mm), and a wet season (October to April, 1364 mm), which coincided with inundation around the tree island site from the nearby Cuiabá river. This tree island site has been the focus of research on soil CO_2 efflux and soil C accumulation [*Carvalho*, 2013], as well as vegetation structure [*Vourlitis et al*., 2015] and soil nutrients [*Vourlitis et al*., 2014]. The site has been described as a succession forest of upland and woodland vegetation with an average leaf area index up to 7.4 m^2 m^{-2} and a mean height of 8 m, dominated not only by the palm *Scheelea phalerata* (Mart.) Bur. (Arecaceae) but also by *Mouriri elliptica* Mart. (Melastomataceae), *Curatella americana* L. (Dilleniaceae), and *Aspidosperma cylindrocarpon* M. Arg. (Apocynaceae) [*Vourlitis et al*., 2015, 2014] (Figure S1 in the supporting information). Measurements made at the site in 2012 showed an accumulation of 21 ton C ha^{-1} y^{-1} of litterfall over the year as 61% leaves, 30% branches, and 9% seed [*Carvalho*, 2013] with large amounts of litterfall accumulated in the dry season (9.11 ton C ha^{-1} $month^{-1}$ in August 2012). Soils were classified as Haplic Eutrofic Planosol [*Couto et al*., 2002] composed of 161 g kg^{-1} of sand, 334 g kg^{-1} silt, 506 g kg^{-1} clay, and 21 g kg^{-1} of soil organic matter at 0–0.10 m depth [*Vourlitis et al*., 2014], with an

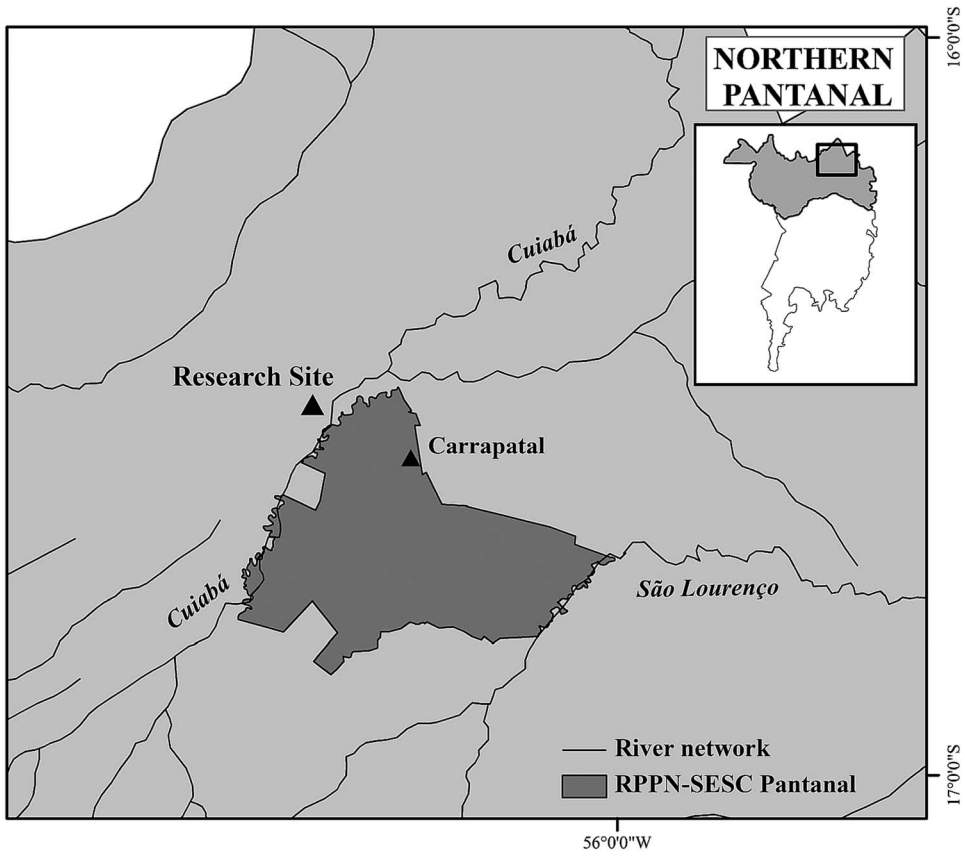

Figure 2. Research site in the Northern Pantanal of Mato Grosso, Brazil, where soil CO_2 concentration was measured in this study and whose soil CO_2 efflux estimates were compared to the results found at another site (Carrapatal) described by *Johnson et al*. [2013] and *Dalmagro et al*. [2016].

average bulk density of 1.35 g cm^{-3} (0–0.30 m depth) and an average root density of 2.75 mg cm^{-3} (0–0.10 m depth) [*Dias*, 2015]. The soil had a pH (measured from a 2:1 slurry of soil:water) in the 4.7–6.8 range depending on the season and an average 57.3 ton C ha^{-1} (0–0.10 m sample) [*Carvalho*, 2013]. While soils in the Northern Pantanal's savanna landscapes are known to be nutrient deficient for the construction of a forest, this particular palm forest showed much greater concentrations of nutrients in the soil compared to other ecosystems nearby: 34 kg P ha^{-1} (deficient), 264 kg K ha^{-1} (deficient), 5473 kg Ca ha^{-1} (surplus), and 2236 kg Mg ha^{-1} (deficient) [*Vourlitis et al*., 2015].

2.2. Multiparameter, Automated In Situ Measurements

Soil oxidation-reduction potential, CO_2 concentrations, volumetric water content (θ), and matric potential (ψ) were measured at both 0.10 m and 0.30 m depths in the soil profile. Soil oxidation-reduction potential was measured using CSIM11 probes (Campbell Scientific Inc., Logan, Utah, USA; accuracy ±0.1%) and placed directly in contact with the soil. While these types of sensors are typically used to measure E_h in solutions, they have also been used to describe electrochemistry of hydric soils [*Vepraskas and Faulkner*, 2000]. Soil CO_2 concentrations were measured with a solid state infrared gas analyzers GMM221 (Vaisala Inc., Helsinki, Finland; accuracy ± (3000 ppm + 2% reading) [*Vaisala*, 2017]) protected with one layer of polytetrafluoroethylene (PTFE) followed by one additional layer of Tyvek sheet prior to installation into the soil, with individual layers sealed with a rubberizing compound. These protective layers prevent water from damaging the sensor while still letting CO_2 gas reach the analyzer with proven results in the field [*Johnson et al*., 2009; *Jassal et al*., 2004]. These PTFE layers were not treated to prevent biofouling, however. Soil water content was measured together with soil conductivity and temperature using GS3 sensors (Decagon Devices Inc., Pullman, Washington, USA; accuracy ±0.03 m^3 m^{-3}, ±1°C), while ψ was measured using MPS2 sensors (Decagon Devices Inc., Pullman, Washington, USA; accuracy ±25% from −5 to −100 kPa, ±1°C). All sensors were

installed into two distinct clusters at 0.10 m and 0.30 m depths contained within an area less than 3 m^2 and with no horizontal replicates. As such, the installation allowed for simultaneous measurements to be made in the soil profile while ensuring no interference between sensor readings. Sensors were connected to a CR1000 data logger equipped with an AM16/32 multiplexer (Campbell Scientific Inc., Logan, Utah, USA) with measurements averaged on a half-hourly basis. The CO_2 modules were turned on for 5 min, once every half hour to prevent localized soil heating [*Johnson et al*., 2013; *Jassal et al*., 2004, 2005] and to save power and maintain autonomy of the system, with soil CO_2 data collected during the on-cycle but after the warm-up period as indicated in the sensor manual. A meteorological station WXT520 (Vaisala Inc., Helsinki, Finland) located about 2 km from the soil sensors provided measurements of precipitation (accuracy ±5%), air temperature (±0.3°C), atmospheric pressure (±0.5 hPa), and relative humidity (±3–5%). Data were collected for 2 years starting 18 October 2013 and ending on 17 October 2015, a period that included the Pantanal's 2014 and 2015 flood cycles (approximately February through May of each year). CO_2 concentration measurements were made almost uninterruptedly. There was a 17 day gap in April 2015 (3 April 2015 to 20 April 2015) due to sensor malfunction, which required sensor replacements at both 0.10 m and 0.30 m depths.

Both CO_2 concentration and oxidation-reduction potential measurements were corrected prior to analysis. The CO_2 readings were corrected for atmospheric pressure and soil temperature following recommendations from Vaisala Inc. (personal communication) shown in equation (1):

$$C = C_M - C_P - C_T \tag{1}$$

where C, C_M, C_P, and C_T (all in ppm) are the corrected, measured, corrected for atmospheric pressure, and corrected for soil temperature soil CO_2 concentrations, respectively, at a given depth. The atmospheric pressure-corrected soil CO_2 concentration, C_P, was calculated following $C_P = K_P \frac{P_a - 1013}{1013}$, where K_P (ppm) = $0.0002C_M + 0.0995$ ($R^2 = 0.997$) and P_a (hPa) is the atmospheric pressure recorded near the research site. The temperature-corrected soil CO_2 concentration (C_T) was calculated following $C_T = K_T \frac{25 - T}{25}$, where K_T (ppm) = $A_0 + A_1 C_M + A_2 C_M^2$, with $A_0 = 5.18 \times 10^{-2}$ ppm, $A_1 = 6 \times 10^{-6}$, and $A_2 = -3 \times 10^{-11}$, and T is the soil temperature (°C) measured alongside the CO_2 module with the MPS2 sensors at 0.10 m and 0.30 m depths. While these corrections are important, they are smaller than the reported accuracy of the CO_2 sensor. For example, at 28°C and 998 hPa, and C_M = 100,000 ppm, values of C_P and C_T would be −0.30 ppm and −0.04 ppm, respectively.

Soil oxidation-reduction potential measurements were made against a saturated K/KCl reference electrode, which requires correction against a hydrogen reference electrode to determine soil E_h values. We follow *Vepraskas and Faulkner* [2000] to obtain E_h (mV) as shown in equation (2):

$$E_h = \mathrm{ORP} - 0.6743T + 213.76 \tag{2}$$

where ORP is the oxidation-reduction potential (mV) measured by the sensor and T (°C) is the soil temperature.

2.3. Soil CO_2 Efflux Calculations

The in situ soil CO_2 concentration and θ measurements were coupled with laboratory measurements of soil CO_2 diffusivity to apply a steady state model to estimate soil CO_2 efflux following steps described in *Tang et al*. [2003], *Baldocchi et al*. [2006], *Vargas et al*. [2010], and *Jassal et al*. [2005]. We first carried out laboratory measurements on intact soil cores to derive a relationship between tortuosity (which includes the soil CO_2 diffusivity) as a function of air-filled porosity in order to select the best model from a suite of published relationships [*Penman*, 1940; *Marshall*, 1959; *Millington and Quirk*, 1961; *Moldrup et al*., 1999] (see Text S1 in the supporting information). Then, using this model, we derived half-hourly values of the soil CO_2 diffusion coefficients from the in situ measurements of θ, which, combined to the automatic station's soil CO_2 concentrations, allowed for an estimate of soil CO_2 efflux every 30 min.

2.3.1. Laboratory Measurement of Soil CO_2 Diffusivity and Tortuosity

Values of soil CO_2 diffusivity (D_s) were obtained in the laboratory using a diffusivity chamber after *Jassal et al*. [2005]. Intact field soil core samples of 0.10 m height and 0.11 m in diameter were taken from the tree island site at 0.05–0.15 m, 0.15–0.25 m, and 0.25–0.35 m depths (three replicates each) representing the depths at, and in between which, the CO_2 sensors were installed. Samples were taken by hitting core samplers directly into the ground so as to obtain an undisturbed sample representative of the depth of interest. Volumetric

water content upon sampling was 0.218 $m^3\ m^{-3}$ (SD = 0.040). The same core samplers were then used in the diffusivity chamber equipped with a CO_2 module GMM221 (Vaisala Inc., Helsinki, Finland) able to measure CO_2 concentrations in the 0–200,000 ppm range and connected to a CR10X data logger (Campbell Scientific, Logan, Utah, USA). A gas mixture of 13% CO_2/Ar was flushed through a 760 cm^3 chamber at 10 L min^{-1} before diffusing through the soil from the bottom of the core samples. Soil CO_2 efflux was measured on the top of the core sample using a LI 6400X gas analyzer (LI-COR Biosciences, Lincoln, Nebraska, USA). The value of D_s was then obtained at steady state following equation (3) [*Jassal et al*., 2005] after 15 min of flushing, as

$$D_s = L\frac{(F_0 + F_L)/2}{C_L - C_0} \tag{3}$$

where L is the core length (0.10 m), F_L (μmol $m^{-2}\ s^{-1}$) is the flux measured at the bottom of the core samples, F_0 (μmol $m^{-2}\ s^{-1}$) is the flux measured at the core surface, and C_L and C_0 (μmol m^{-3}) are the CO_2 concentrations measured by the CO_2 module and the gas analyzer, respectively. A correction is made following equation (4) to separately account for the efflux produced by the soil core sample [*Jassal et al*., 2004]:

$$F_L = F_0 - F_S \tag{4}$$

where F_S (μmol $m^{-2}\ s^{-1}$) is the CO_2 efflux generated by the soil core sample that was measured prior to using the diffusivity chamber by capping the bottom of the core. Diffusion measurements were made at various levels of θ obtained by differential weighing of the core samples with typical values in the range of $7.97 \pm 0.22 \cdot 10^{-6}\ m^2\ s^{-1}$ and $7.26 \pm 0.21 \cdot 10^{-5}\ m^2\ s^{-1}$ in dry soil. Values of D_s ($m^2\ s^{-1}$) were then used to calculate tortuosity in equation (5):

$$D_s = \xi D_a \tag{5}$$

where ξ (dimensionless) is the tortuosity factor (described below), and D_a ($m^2\ s^{-1}$) is the diffusion coefficient of CO_2 in free air and defined as per equation (6) [*Tang et al*., 2003]:

$$D_a = D_{a0}\left(\frac{T}{293.15}\right)^{1.75}\left(\frac{P_a}{1013}\right) \tag{6}$$

where T (K) is the air temperature, P_a (hPa) atmospheric pressure, and D_{a0} is $14.7 \times 10^{-6}\ m^2\ s^{-1}$ as the reference value of D_{a0} at reference conditions (293.15 K, 1013 hPa).

The tortuosity factor has been studied as a function of air-filled porosity (α, $m^3\ m^{-3}$) with many proposed relationships described and tested in Text S1. Air-filled porosity was calculated following equation (7):

$$\alpha = \varphi - \theta = 1 - \frac{B}{2.65} - \theta \tag{7}$$

where θ ($m^3\ m^{-3}$) is the volumetric water content, φ ($m^3\ m^{-3}$) is the soil's porosity, and B (g cm^{-3}) is the soil core's bulk density. Four tortuosity models as a function of air-filled porosity were tested (Table S1 and Figure S2 in the supporting information) with two models showing a reasonable fit: *Millington and Quirk* [1961] with R^2 = 0.51 (RMSE = 0.01) and *Moldrup et al*. [1999] with R^2 = 0.45 (RMSE = 0.01). All models showed much lower tortuosity with increasing air-filled porosity than the fitted data with a power function ($\xi = 0.794\alpha^{1.97}$, R^2 = 0.63).

2.3.2. Soil CO_2 Efflux Calculation From the Automatic Station Measurements

The laboratory measurements confirmed the relationship between ξ and α (Text S1), which we used as the starting point for calculating half-hourly soil CO_2 efflux estimates. First, θ measurements from the automatic station at both 0.10 m and 0.30 m were used to obtain α (from equation (7)) and ξ at both depths using the models from *Millington and Quirk* [1961] and *Moldrup et al*. [1999]. These half-hourly values of ξ were then used to derive D_s at 0.10 m and 0.30 m depth at the research site by combining equations (5) and (6) using soil temperature measurements. Soil CO_2 efflux was then estimated following steps described by *Johnson et al*. [2013] using the flux gradient method [*Vargas et al*., 2010; *Tang et al*., 2003] by first calculating CO_2 fluxes at the 0.05 and 0.20 m depths using Fick's law of diffusion as shown in equation (8) and obtained using the in situ measurements of soil CO_2 concentrations at 0.10 m and 0.30 m in the soil:

$$F_z = -D_s\frac{dC}{dz} \tag{8}$$

where F_z is the CO_2 efflux (μmol m^{-2} s^{-1}) at depth z (m) determined from the CO_2 concentration gradient (dC/dz) with C as the corrected CO_2 concentration (μmol m^{-3}) and the diffusivity D_s (m^2 s^{-1}) of CO_2 in the soil profile. We then computed the surface flux (F_0 at $z = 0$, i.e., soil efflux) following *Baldocchi et al*. [2006] shown in equation (9):

$$F_0 = \frac{z_{i+1}F_i - z_iF_{i+1}}{z_{i+1} - z_i} \tag{9}$$

using z_{i+1} and z_i as 0.20 m and 0.05 m, respectively, with the CO_2 concentrations measured with the sensors installed at 0.10 m and 0.30 m depths for $F_{0.20}$ (obtained from equation (8) and using an average D_s from values obtained at 0.10 m and 0.30 m) and surface CO_2 concentrations and soil CO_2 concentration at 0.10 m depth for $F_{0.05}$ (obtained from equation (8) using D_s derived at 0.10 m depth). CO_2 concentration at the soil surface was assumed to be 400 ppm.

Values of F_0 were validated using a portable soil respiration system (PP Systems model EGM4). Despite a deviation between modeled (with the sensors in the soil) and measured values of F_0 (Figure S3), we considered the model to be validated due to the large error bars associated with the estimates (as systematic error discussed in section 3.4). Soil CO_2 concentrations measured at 0.10 m were corrected by adding 1500 ppm to all measured values to correct in situ sensor measurements with field-based efflux measurements. This correction was necessary to prevent negative efflux estimates due to the large error in the sensor measurements when soil CO_2 concentrations approached atmospheric levels (Text S1). Negative effluxes were never measured in the field, and the modeled estimates of a negative F_0 resulted from large concentration gradients between the soil surface and the 0.10 m depth leading to $F_{0.05} > F_{0.20}$ (see equation (9)). Any remaining negative F_0 estimates following the offset correction were removed from the time series. We also tested two additional levels of surface CO_2 concentrations (1000 ppm and 2000 ppm) to check the model's sensitivity (see Table S2). The *Moldrup et al*. [1999] model including the offset with an assumption of 400 ppm CO_2 at the surface showed the validation outcome with RMSE = 0.044 mg CO_2-C m^{-2} s^{-1} (n = 13; Figure S2). A total of 26,712 estimates of F_0 were available when applying this tortuosity model (76% model coverage for the full times series) with missing data resulting from sensor malfunction, removal of negative values, and periods when the soil diffusivities could not be calculated due to soil conditions at field capacity.

2.4. Soil Water Flows

2.4.1. Separation of Periods Based on Precipitation

We separate the time series into three periods—wetting-up, wet, and dry—based on anomalous accumulation of precipitation previously used to determine crop planting dates [*Arvor et al*., 2014; *Liebmann et al*., 2007] from the precipitation data collected from the automatic station. Here we compare annual precipitation accumulation against annual average precipitation following equation (10):

$$AA(t) = \sum_{n=1}^{t} (P(n) - P_{\text{mean}}) \tag{10}$$

where $AA(t)$ is the anomalous accumulation (mm) at day t, $P(n)$ (mm) is the precipitation accumulated from the first day of the series, and P_{mean} (mm) is the annual average precipitation measured for each year (1684.5 mm y^{-1} in 2013–2014 and 1423.9 mm y^{-1} in 2014–2015). Periods are then assigned using minimum and maximum $AA(t)$: the period prior to minimum $AA(t)$ was designated as the wetting-up period, while the period following maximum $AA(t)$ was labeled as the dry period. The phase between minimum and maximum $AA(t)$ was designated as the wet period. These phases were assigned for both 2013–2014 (henceforth as 2014 flood cycle) and 2014–2015 (henceforth as 2015 flood cycle) with minima $AA(t)$ occurring on 11 November 2013 and 11 November 2014 and maxima on 23 May 2014 and 4 May 2015, respectively (Text S2 and Figures S7 and S8).

2.4.2. Water Flow in the Soil

We used Darcy's law to estimate the flow of water in the soil between the 0.10 m and 0.30 m depths through a water potential gradient as shown in equation (11) [*Campbell and Norman*, 1998]:

$$J = -K(\psi)\frac{d\psi}{dz} \tag{11}$$

where J is the soil water flux (cm d^{-1}), $K(\psi)$ is the soil hydraulic conductivity as a function of water potential (cm d^{-1}), and $d\psi/dz$ is the daily average water potential gradient derived from the two depths (0.10 m and

0.30 m) and estimated as $\frac{0.30\psi_{0.30}-0.10\psi_{0.10}}{0.20}$, with $\psi_{0.30}$ and $\psi_{0.10}$ representing the hydraulic head (in m) at the 0.30 m and 0.10 m depths.

We determined $K(\psi)$ using a HYPROP® system (UMS GmbH, Munich, Germany), which uses vertically aligned tensiometers with ceramic cups to take soil matric potential measurements as water evaporates from a soil sample [*Schindler et al*., 2010]. Intact field soil samples were obtained from the research site using 250 cm^3 stainless steel cores (0.08 m diameter, 0.05 m height) representing the 0.20–0.25 m layer (depth between the two water potential sensors described above). Both ends of the core sample were trimmed and capped with plastic lids for transportation. In the laboratory, the lids were removed from the sample, a fine mesh applied at one end, and let to saturate for 24 h in a pan of water. The HYPROP® sensor head and tensiometers (bottom and top) were refilled with distilled water manually using a syringe and allowed to sit for 24 h to degas. After degassing, two holes for each tensiometer were drilled in the saturated soil sample with the auger and template provided with the HYPROP®. The sample was then mounted onto the HYPROP® sensor head with the tensiometers in place and set on a scale. Both the HYPROP® device and the scale were connected to a computer running the tensioView® software (version 1.10) to track changes in soil mass, tension, and evaporation. Measurements were concluded once air entered the ceramic cup of the tensiometers and tension dropped to 0 kPa (after 11 days). The soil was then removed from the sample core and dried in a 105°C oven for 24 h before measuring dry mass. The soil dry mass was entered in the HYPROP-FIT software to calculate θ. The soil retention curve and unsaturated conductivity were determined by fitting the data to the unimodal constrained model of *Van Genuchten* [1980] and *Mualem* [1976], respectively. The results allowed an estimate of $K(\psi)$ (cm d^{-1}) as a function of tension (pF as $\log\psi$ with ψ in cm following 10.197 cm kPa^{-1}) such that $\log K(\psi) = -2.93pF + 5.25$ ($R^2 = 0.99$, $p < 0.01$). For each half-hourly field measurement of ψ, we obtained values for $K(\psi)$ at 0.10 m and 0.30 m and used a mean value to estimate soil water flux using Darcy's law. Results from the above experiment also provided the 0.20–0.25 m depth field capacity of 0.388 m^3 m^{-3}.

All soil CO_2 efflux results are provided in g CO_2-C m^2 s^{-1} after conversion of μmol CO_2 m^{-2} s^{-1}. Data analyses were performed using statistical software R (v.3.3.1) [*R Core Team*, 2016] in RStudio (v.0.99.902) and using the *openair* package v.1.8.6 [*Carslaw and Ropkins*, 2012, 2016], graphics using *ggplot2* [*Wickham*, 2009], *gridExtra* v.2.2.1 [*Auguie*, 2016], *scales* v.0.4.0 [*Wickham*, 2016], and *grid* [*R Core Team*, 2016] with R source code available at https://github.com/mlathuilliere/Lathuilliere_SI_JGR.git. Measured data and modeled results are publicly available at https://github.com/UBCecohydro/data.public.

3. Results and Discussion

3.1. Seasonal Soil CO_2 Concentration and Efflux

Mean soil CO_2 concentrations were significantly different between the 2014 and 2015 flood cycles at both 0.10 m ($F = 8.85$; $p < 0.001$) and 0.30 m depth ($F = 1.58$; $p < 0.001$) with maxima close to 200,000 ppm at 0.30 m depth in February and March 2014 (Figure 3). This concentration is close to the detection limit of the CO_2 sensor, which was briefly exceeded in March 2014 (90 measurements). Soil CO_2 concentrations increased with depth, with mean values for the 2014 flood cycle of 23,808 ± 3476 ppm at the 0.10 m depth (±propagated measurement errors from instrumentation) and 66,060 ± 4321 ppm at the 0.30 m depth ($F = 0.45$; $p < 0.001$). Median values were 5630 ± 3113 ppm and 46,370 ± 3927 ppm for the 0.10 m and 0.30 m depths, respectively. For the 2015 flood cycle, mean concentrations were 6459 ± 3129 ppm and 40,830 ± 3817 ppm with median values of 987 ± 3020 ppm and 16,620 ± 3332 ppm for the 0.10 m and 0.30 m depths, respectively ($F = 0.081$; $p < 0.001$). The sometimes tenfold increases in mean soil CO_2 concentrations between 0.10 m and 0.30 m were attributed to limitations in CO_2 diffusion deeper in the soil [*Hashimoto and Komatsu*, 2006], while decomposition of litterfall and root activity are typically more prevalent at shallower depths [*Jobbágy and Jackson*, 2000]. The tree island site is home to a tall palm forest (Figure S1), which provides 21 ton C ha^{-1} y^{-1} of litterfall to the soil [*Carvalho*, 2013] expected to remain at shallow soil depths [*Hashimoto and Komatsu*, 2006]. However, despite a shallow root density of 2.75 mg cm^{-3} (at 0–0.10 m depth from *Dias* [2015]), we also expect deeper roots to contribute to soil CO_2 production via root respiration. Mean soil CO_2 efflux at the site could not be estimated with precision using the gradient method due to the propagation of systematic and random instrumental error terms or due to nonsteady state conditions arising from an abrupt surge in θ values. The mean annual soil efflux was estimated

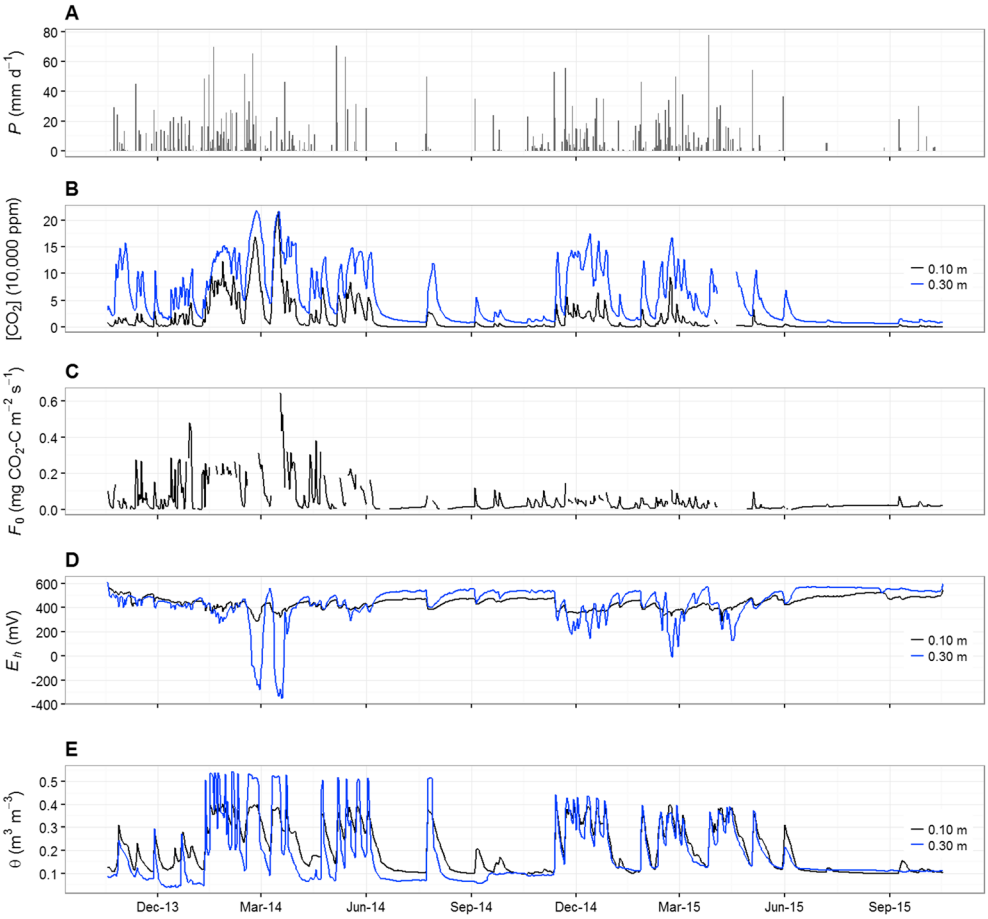

Figure 3. Data collected and modeled between 18 October 2013 and 17 October 2015 at the tree island site: (a) daily total precipitation (P, mm d^{-1}); (b) daily mean soil CO_2 concentration ([CO_2], 10,000 ppm); (c) modeled daily mean soil CO_2 efflux (F_0, mg CO_2-C m^{-2} s^{-1}); (d) daily mean soil oxidation-reduction potential (E_h, mV); (e) daily mean volumetric soil water content (θ, m^3 m^{-3}).

0.046 ± 0.102 mg CO_2-C m^{-2} s^{-1} (median: 0.0181 ± 0.0748 mg CO_2-C m^{-2} s^{-1}) with a 2014 flood cycle mean of 0.074 ± 0.100 mg CO_2-C m^{-2} s^{-1} on 70% of modeled data (median: 0.0179 ± 0.0632 mg CO_2-C m^{-2} s^{-1}) and a 2015 mean of 0.023 ± 0.103 mg CO_2-C m^{-2} s^{-1} on 83% of modeled data (median: 0.0181 ± 0.0804 mg CO_2-C m^{-2} s^{-1}).

Soil CO_2 concentration varied with the hydrologic period (Table 1) defined as wetting-up, wet, and dry periods based on anomalous accumulation of precipitation (Figures S7 and S8). Statistical analysis showed significant differences between periods from 2013 to 2015 at both 0.10 m (F = 2540; $p < 0.001$) and 0.30 m depth (F = 3974, $p < 0.001$). Mean CO_2 concentrations were typically greater in the wet period, while wetting-up and dry periods showed similar CO_2 concentrations at the 0.10 m and 0.30 m depths (Table 1). Again, differences in soil CO_2 effluxes with hydrologic period were not discernible due to instrumental error terms and possible deviation from nonsteady state conditions when the soil experienced frequent saturation events with large swings in soil CO_2 concentrations, especially during the 2014 flood cycle (Table 1). Soil efflux estimates changed by about ±2 to 55% when the CO_2 surface concentration in the model was increased to 1000 ppm (in equations (8) and (9)) and by about ±10 to 160% when increasing the value to 2000 ppm (Table S2). Monthly total soil efflux values at the site are available in Table S3.

Mean annual soil CO_2 efflux in the 2015 flood cycle was similar to the mean of 0.0410 mg CO_2-C m^{-2} s^{-1} obtained monthly (one observation per month) at the same location during the 2012 calendar year [*Carvalho*, 2013] and to the mean of 0.0424 mg CO_2-C m^{-2} s^{-1} obtained at a nearby tree island ("Carrapatal" in Figure 2) [*Johnson et al.*, 2013]. Together, these values (Table 2) comprise the interannual

Table 1. Soil Saturation Frequency (% Measurements Within Period), Mean Soil CO_2 Concentration Measured ([CO_2]), and Soil CO_2 Efflux (F_0) Estimated Using the Gradient Method at the Tree Island Site for the 2014 and 2015 Flood Cycles. Values Are Represented With an Error Estimate Obtained by Propagating Measurement Errors From the Sensors

	2014 Flood Cycle			2015 Flood Cycle		
	Wetting-Up	Wet	Dry	Wetting-Up	Wet	Dry
Soil saturation frequency (%) (at 0.10 m; 0.30 m)	(0; 0)	(8; 22)	(1; 7)	(0; 0)	(6; 12)	(0; 0)
[CO_2] (ppm) 0.10 m	7,647 (±3,153)	39,580 (±3,792)	6,434 (±3,129)	1,413 (±3,028)	13,040 (±3,261)	1,189 (±3,024)
[CO_2] (ppm) 0.30 m	81,850 (±4,637)	90,260 (±4,805)	32,110 (±3,642)	12,410 (±3,248)	72,480 (±4,450)	15,120 (±3,302)
F_0 (mg CO_2-C m^{-2} s^{-1})	0.0484 (±0.0351)	0.121[a] (±0.073)	0.022 (±0.139)	0.032 (±0.132)	0.0278 (±0.036)	0.0177 (±0.148)

[a]Value obtained under nonsteady state conditions (see discussion in section 3.4).

and spatial variability in soil CO_2 efflux in the Northern Pantanal region as presently known, varying by soil type, local organic matter, and duration of soil saturation [*Johnson et al*., 2013; *Couto and Oliveira*, 2011].

3.2. Soil Water Saturation and CO_2 Dynamics

Soil wetting and drying events were important drivers of temporal dynamics in soil CO_2 concentrations and efflux. Mean soil temperature was 27°C (SD = 2°C) at both the 0.10 m and 0.30 m depths with very weak correlations between soil temperature and CO_2 concentrations and soil temperature and soil CO_2 efflux ($R^2 = 0.01$, $p < 0.01$ in both cases). As such, we expect soil CO_2 dynamics at the tree island site to be primarily controlled by soil water dynamics, expressed in terms of soil volumetric water content (θ) and soil matric potential (ψ) (Figure 4) [*Johnson et al*., 2013]. Given the large variability in θ during the 2014 and 2015 flood cycles, we define soil saturation events when values of θ were greater than field capacity (0.388 m^3 m^{-3}), which coincides with the maximum level above which we were unable to model soil CO_2 diffusivities (and by extension F_0) from the laboratory experiment. Soil at the 0.10 m and 0.30 m depths was saturated 4% and 10% of the time, respectively, with greater concentration of saturation events in the wet periods of the 2014 and 2015 flood cycles (Table 1 and Figure 3) also confirmed with values of E_h measured at both depths.

Both 2014 and 2015 flood cycles showed similar annual average values of E_h with a mean of 442 mV (SD = 48) and 444 mV (SD = 145) at the 0.10 m and 0.30 m depths, respectively. The larger seasonal differences were apparent in the February–March period, especially considering differences from the wetter (2014) versus drier (2015) year based on precipitation, inundation period, and the stage of the nearby Cuiabá river (Table 2). The February–March 2014 period showed a strongly negative E_h at 0.30 m depth (<-300 mV) (Figure 3), indicative of anoxic conditions. Negative E_h values occurred twice in 2014: 22 February 2014 to 2 March 2014 with a minimum value of -323 mV and 13 March 2014 to 21 March 2014 with a minimum E_h of -372 mV, suggesting longer periods of θ greater than field capacity. This extended period of negative E_h was not observed in the 2015 flood cycle, suggesting absence of long-term saturation of the soil at the tree island during the drier year. The short periods of $E_h < -300$ mV at the site in the 2014 flood cycle also created

Table 2. Mean Annual and Total Soil CO_2 Efflux (F_0) Reported for the Research Site and the Nearby Carrapatal Tree Island Shown in Figure 2. The F_0 Values in This Study Are Represented With an Error Estimate Obtained by Propagating Measurement Errors From Instrumentation

Site[a]	Research Site	Research Site	Research Site	Carrapatal
Period	2012	2013–2014	2014–2015	2008–2010
Precipitation Jan–Mar (mm)	594	695	577	356/357
Inundation (days)[b]	102	160	193	160/152
Maximum height of Cuiabá River (m)[c]	4.02	4.75	4.32	4.45/4.55
Mean F_0 (mg CO_2-C m^{-2} s^{-1})	0.0410[d]	0.074 ± 0.100	0.023 ± 0.103	0.0424
Total F_0 (g CO_2-C m^{-2} y^{-1})	1293	1630 ± 2190[e] (70% of data)	593 ± 2690 (85% of data)	1220
Reference	[*Carvalho*, 2013]	This study	This study	[*Johnson et al*., 2013]

[a]The tree island site was reported to have 57 ton C ha^{-1} [*Carvalho*, 2013] (0–0.10 m depth); the Carrapatal site has 14 ton C ha^{-1} [*Johnson et al*., 2013] (0–0.20 m depth).
[b]Length of inundation determined as a function of the height of the Cuiabá River according to *Girard et al*. [2010].
[c]Data obtained from SESC (personal communication) near the tree island site.
[d]Measurements made at the same study site using an EGM4 infrared gas analyzer (PP Systems, UK).
[e]Value obtained under nonsteady state conditions (see discussion in section 3.5).

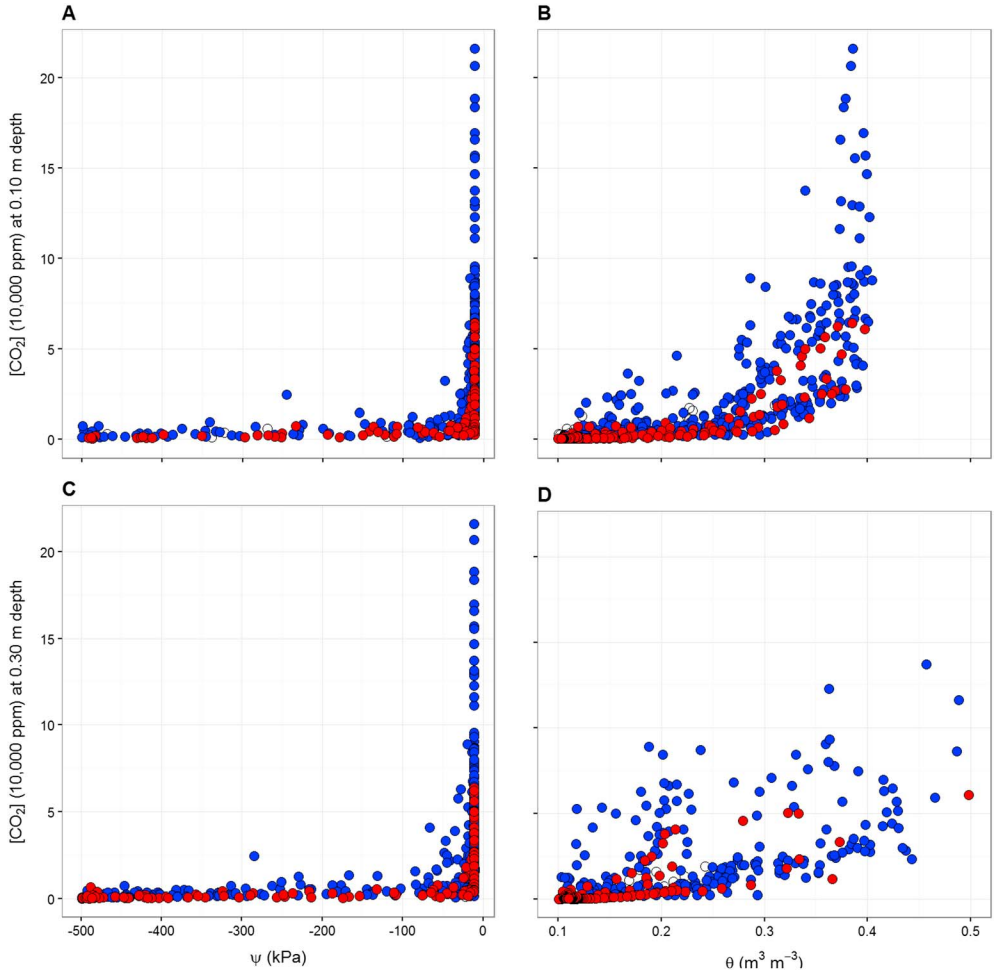

Figure 4. (a and c) Relationship between soil CO_2 concentration ([CO_2], 10,000 ppm) and soil water potential (ψ, kPa) and (b and d) soil volumetric water content (θ, $m^3\ m^{-3}$) at 0.10 m and 0.30 m depths for the wet-up (open), saturated (blue), and dry periods (red) between 2013 and 2015 at the tree island.

conditions in which CO_2 could be reduced to CH_4 [*Vepraskas and Faulkner*, 2000]. Measurements made in 2010 and 2011 at the Carrapatal site (Figure 2) showed $E_h < -200$ mV [*Messias et al*., 2013] resulting from soil saturation during flooding. The Carrapatal site exhibited $E_h < 0$ for 23 days in 2013, and for 63 days in 2014, with differences linked to longer inundation periods for 2014 compared to 2013 [*Dalmagro et al*., 2016]. Given the much shorter time of anoxic conditions in the present study, we also conclude that soil saturation at the 0.30 m depth was highly episodic and of short duration, as shown by the transition from strongly reducing back to oxidizing conditions in the E_h profile (Figure 3).

Soil CO_2 concentrations increased with θ at both the 0.10 m and 0.30 m depths (Figures 4b and 4c) with a similar relationship observed with soil CO_2 efflux (Figure S10). During the wet periods, soil almost always had greater CO_2 concentrations (Figure 3). Wetting events, whether caused by local precipitation, regional flooding, or both, created ψ values at or near saturation and restricted CO_2 diffusivity conditions, which allow CO_2 to accumulate in the soil [*Jassal et al*., 2005; *Johnson et al*., 2013]. In the wet periods, soil CO_2 diffusion coefficients calculated from the tortuosity obtained with the *Moldrup et al*. [1999] model typically dropped in the wet period (see Figures S5 and S6) when θ approached field capacity (note that in events of $\theta > 0.388\ m^3\ m^{-3}$ (field capacity), values of D_s could not be calculated). Reduced precipitation and shorter duration of flooding near the tree island in the 2015 flood cycle created conditions in which the soil was only occasionally saturated (6% and 12% of the wet period at the 0.10 m and 0.30 m depths, respectively; Table 1 and Figures S7 and S8). These observations echo those of *Hashimoto and Komatsu* [2006], who noted that soil CO_2 concentrations increased with CO_2 production and decreasing soil CO_2 diffusivity, thereby affecting the

efflux. This information provides additional uncertainty on processes during the wet period of 2014 when the soil CO_2 effluxes were the highest in the time series, which also coincided with a period when we believe that steady state conditions were not met in the soil (>0.200 mg CO_2-C m^{-2} s^{-1}, Figure 3).

3.3. Soil Water Fluxes and CO_2 Dynamics

Analysis of soil water fluxes provided further insights into soil biogeochemistry at the site. The annual mean soil hydraulic conductivity $K(\psi)$ was 5.22×10^{-2} cm d^{-1}, with a mean water flux (J) of 0.11 cm d^{-1} (SD = 0.12). Average J values for the periods of negative E_h were 0.19 cm d^{-1} for 22 February 2014 to 2 March 2014 and 0.15 cm d^{-1} for 13 March 2014 to 21 March 2014. In 2015, soil saturation was less frequent (6% and 22% of the wet period at the 0.10 m and 0.30 m depths, respectively) and, more importantly, much shorter lived as demonstrated by a mostly positive E_h throughout the year. A drier 2015 resulted in decreased CO_2 concentration buildup at the 0.10 m depth with a much smaller $F_{0.05}$, thereby reducing the efflux from the steady state model (equation (9)). Similarly, precipitation events occurring in the dry period such as on 23 July 2014 (12 mm d^{-1}) and on 24 July 2014 (50 mm d^{-1}) led to soil CO_2 concentrations of 1281 ± 3026 ppm and 17,970 ± 3359 ppm at the 0.10 m depth (daily mean) with a mean daily soil CO_2 efflux of 0.030 ± 0.144 mg CO_2-C m^{-2} s^{-1} and 0.0748 ± 0.0783 mg CO_2-C m^{-2} s^{-1}, respectively. Such a rainfall event can generate not only a CO_2 "pulse" due to sudden microbial activity following soil wetting (also known as the "Birch" effect [*Jarvis et al*., 2007]) but also physical mechanisms that include changes in the soil diffusion coefficient and physical displacement of CO_2 from soil pore space [*Kim et al*., 2012]. The length of dry conditions in the soil combined to the intensity and length of precipitation events can influence the magnitude of these pulses, thereby affecting net ecosystem exchange depending on how the ecosystem's photosynthetic activity responds to the precipitation event [*Jarvis et al*., 2007; *Huxman et al*., 2004]. An irrigation experiment in a burnt Spanish pine forest showed soil CO_2 efflux pulses as high as 0.28–0.48 mg CO_2-C m^{-2} s^{-1}, which are similar to the pulse estimated at the research site in the 2014 wet period [*Marañón-Jiménez et al*., 2011]. Similarly, *Lee et al*. [2004] report an average ecosystem flux of 0.263 mg CO_2-C m^{-2} s^{-1} during Hurricane Floyd in 1999, with an irrigation experiment confirming CO_2 pulses as high as 0.144 mg CO_2-C m^2 s^{-1} (August 2002) [*Lee et al*., 2004]. We therefore expect a difference between the 2014 and 2015 flood cycles as the numbers of 30 min precipitation events greater than 5 mm were of 320 and 77, respectively. These events, in addition to a likely temporary rise in the water table in February–March 2014 as shown by measurements of E_h, further contributed to the differences in soil CO_2 effluxes observed at the research site between the flood cycles.

Negative E_h values at the 0.30 m depth are indicative of extended soil saturation, and therefore, we use these $E_h < 0$ events to estimate water fluxes via deep percolation to highlight annual hydrological processes and further link C and water cycles (Figures S7 and S8). During the wet period, the mean daily soil water flux was 0.12 cm d^{-1} in both 2014 and 2015 flood cycles, reaching 0.18 cm d^{-1} when $E_h < 0$. Average daily evapotranspiration (ET) obtained by the MODIS ET product [*Mu et al*., 2011] validated for Central-Western Brazil [*Loarie et al*., 2011] and extracted using R statistical software [*R Core Team*, 2016] with packages *date* [*Therneau et al*., 2014], *sp* [*Bivand et al*., 2013; *Pebesma and Bivand*, 2005], *rgdal* [*Bivand et al*., 2014], and *raster* [*Hijmans*, 2014] (Text S3) showed values above 4.0 mm d^{-1} between November 2013 and April 2014 (Figure S9). This estimate is provided for 1 km^2 at the location of the tree island site and is believed to be representative of the landscape and the vegetation. Annual precipitation for the September 2013 to August 2014 period was 1684 mm y^{-1}, with ET generally lower than precipitation in all months, suggesting that the site was not water limited annually. Annual ET was 1083 mm y^{-1} (Table S4). During the 2014 flood cycle, the month of March experienced 149 mm $month^{-1}$ of precipitation compared to 139 mm $month^{-1}$ of ET. With saturated soils from precipitation and flood waters at the site, ET was over twice our estimates of soil water drainage (J), suggesting that ET could be an important control on soil water status and hence be a strong influence on soil CO_2 concentration and efflux at the tree island site. In short, we highlight an important connection between the C and water cycles: while precipitation events potentially favor CO_2 efflux through pulses, ET and deep percolation at the site rapidly reduce θ and, by extension soil CO_2 concentrations and effluxes, only maintained under extended saturation conditions during the short flood event of 2014.

The above results provide insight into ecohydrological and topographic controls on soil water processes, which, in turn, impact soil CO_2 concentrations and effluxes. Unlike the research site that contains a palm

Table 3. Comparison of Flooding, Precipitation (P), and Evapotranspiration (ET) as Estimated by MOD16 [*Mu et al*., 2011] and Days With Negative Oxidation-Reduction Potential (E_h) for Two Tree Islands in the Northern Pantanal (Figure 2)

Tree Island Considered	Flooding	P (mm y^{-1})	ET (mm y^{-1})	$E_h < 0$ (Days)	Dominant Water Input
This study 2013–2014	None	1684	1083	16 (2 × 8)	P
This study 2014–2015	None	1424	No data[a]	2	P
Carrapatal 2013–2014	Full	1049–1525[b]	1459	63	Inundation

[a]Data not available at the time of writing.
[b]2010–2012 range as data for 2014 was incomplete.

forest, the Carrapatal site (Figure 2) is not a forest but an invasion front containing a mix of species [*Dalmagro et al*., 2016]. Vegetation and topography at the research site favor rapid drying of the soil due to greater ET and deep drainage in the palm forest, especially when the soil was saturated in March 2014. Both research and Carrapatal sites were not water limited in 2014, although the Carrapatal site had a greater annual ET of 1459 mm y^{-1} (Table 3). In 2013–2014, the Carrapatal site was completely flooded with $E_h < 0$ for 63 days, longer than previous years [*Dalmagro et al*., 2016] with daily ET similar to our site for the February to April 2014 timeframe (4.1–4.3 mm d^{-1}). We therefore expect deep percolation to be within a similar range of 1.8 mm d^{-1} such that ET becomes an important control to reduce the flood waters with likely more evaporation than transpiration due to flooding and the predominance of younger, smaller trees. In contrast to our site, the flooded Carrapatal site may also lose more C in its dissolved form: DOC concentrations near the Carrapatal site were between 4 and 12 mg L^{-1} with the lowest concentrations recorded at the height of the flood season [*Dalmagro et al*., 2013]. Moreover, the prolonged inundation period and anoxic conditions when $E_h < 0$ (for similar soil pH) suggest a likely reduction of CO_2 into CH_4 [*Vepraskas and Faulkner*, 2000] and likely production of CH_4 through methanogenesis, which merits further investigation. These geographical differences in precipitation and flooding at the two sites express the complexity in assessing the C balance in the Pantanal biome in time and space (Tables 2 and 3), as well as the geographic and environmental drivers that could influence soil CO_2 efflux throughout the annual flood cycles, despite similar soil water mechanisms.

3.4. Challenges in Estimating Soil CO_2 Efflux in the Pantanal

This research uses the well-established gradient method for determining soil CO_2 efflux with the benefit of providing high temporal resolution. However, while the method has been used successfully in the Pacific Northwest [*Jassal et al*., 2004, 2005] and California [*Baldocchi et al*., 2006], additional challenges were apparent for its application in the Pantanal. We consider the total error in the values of F_0 as the sum of systematic and random errors [*Richardson et al*., 2006]. The systematic error was propagated as uncertainty in F_0 derived from measurement error associated with the instrumentation used at the research site. The largest systematic errors in F_0 came from the uncertainty in soil CO_2 concentrations of ± (3000 ppm + 2% reading), especially for soil CO_2 values closer to atmospheric CO_2 concentrations. Similar sensors with smaller concentration measurement ranges (e.g., 0–10,000 ppm) have been used widely in research using the gradient methods [*Cueva et al*., 2015; *Vargas et al*., 2010; *Baldocchi et al*., 2006; *Jassal et al*., 2005; *Tang et al*., 2003] with an accuracy of ± (20 ppm + 2% reading). Future research in the Pantanal should consider additional sensors in the topsoil able to measure soil CO_2 concentration at similar ranges and with greater accuracy. Moreover, many sites in the Pantanal can experience either repeated saturation events such as the tree island at the research site in 2014, or full inundation for several months of the year when CO_2 concentrations can exceed the 200,000 ppm sensor limit used in this study (e.g., as seen in *Couto et al*. [2012]). These conditions complicate the choice of the sensor ranges to be used in the gradient method and the accuracy accompanying the choice of such sensors.

Random errors in the values of F_0 are expected in cases of large changes in environmental conditions [*Cueva et al*., 2015], as seen during the rapid saturation and drying of the soil in the February–March 2014 period, which we believe affected our model's steady state assumption. For every 30 min estimate of F_0, we have assumed a constant CO_2 flux between our two selected depths (as $F_{0.05}$ and $F_{0.20}$ in equation (9)), which might not hold all the time. Rapid wetting and drying events at the tree island infer equally dynamic changes in soil CO_2 concentrations and diffusion in the top 0.30 m of soil. These differences can be expected at other sites in the Pantanal, which has a highly diverse landscape, soil, and soil water dynamics during annual flood

pulses [*Nascimento et al*., 2015]. Moreover, large changes in environmental conditions might be accompanied by additional processes unaccounted for in the steady state model, namely, the physical transfer of CO_2 out of the soil during precipitation events when water can rapidly occupy soil pores, thereby pushing out CO_2 [*Kim et al*., 2012; *Huxman et al*., 2004] or additional release of CO_2 dissolved in precipitation during rain events [*Lee et al*., 2004]. Should these processes be significant at 0.30 m depth, they not only would have an effect on soil CO_2 concentrations at 0.10 m (affecting the CO_2 concentration gradient) but would also introduce additional uncertainty in the interpretation of increased soil CO_2 concentrations at 0.10 m depth with CO_2 production, soil CO_2 diffusivity, and precipitation inputs [*Hashimoto and Komatsu*, 2006].

4. Conclusion

This study's half-hourly measurements of soil CO_2 concentrations, modeled efflux values, and measured oxidation-reduction potential for two inundation cycles in the Pantanal provided insight into the dynamics driving the C cycle in the tropical wetland. The Pantanal's topography results in slow soil water drainage, which, with local precipitation and regional flooding, create conditions in which soil CO_2 effluxes are decreased due to a decrease in diffusivity. Soil CO_2 concentrations were strongly influenced by precipitation events during the annual flood cycle with a wetter 2014 flood cycle showing much larger soil CO_2 concentrations than the drier 2015 flood cycle. Rapid changes in soil water content were attributed in part to soil drainage, but ET of the palm forest appeared to be a stronger driver of soil water depletion. The presence or absence of a forest along with the topography and probability of flooding can greatly impact C dynamics. There is also a trade-off in soil CO_2 emissions with inundation and soil saturation: inundation can reduce soil CO_2 effluxes, but the magnitude depends greatly on the length of the inundation cycle. Our results further highlight the spatial-temporal complexity of the C balance in the Pantanal, which should be considered in further studies on this wetland of international importance.

Acknowledgments

This work was carried out under the auspices of the Brazilian National Institute for Science and Technology in Wetlands (Instituto Nacional de Ciência e Tecnologia em Áreas Úmidas, INCT-INAU) supported by the Brazilian Conselho Nacional de Desenvolvimento Científico e Tecnológico (CNPq, process 573990/2008-5). The authors acknowledge CNPq for additional funding through the Bolsa de Desenvolvimento Tecnológico Industrial DTI 2 (382983/2012-2 and 383389/2013-5 to M.J.L.). We are grateful to the Brazilian Social Service of Commerce SESC Pantanal for access to the field site and support from the park rangers. Additional thanks are owed to Paula Carvalho, Edna Maria de Souza Carneiro, and Marizeth de França Dias for sharing field measurements. We are thankful for laboratory space and equipment provided by Francisco de Almeida Lobo and Carmen Eugenia Rodríguez Ortíz at the Universidade Federal de Mato Grosso, as well as transportation and logistical support from Ricardo Santos Amorim and Suzana Souza dos Santos. Special thanks are owed to George Vourlitis for discussions and additional comments on results. Finally, we acknowledge the very helpful comments from the reviewers, editor, and associate editor, which resulted in a significant improvement in the quality and organization of this paper. Field measurements obtained for this study are available in the following public repository: https://github.com/UBCecohydro/data.public. The R script used to perform the calculations can be found at https://github.com/mlathuilliere/Lathuilliere_SI_JGR.git.

References

Arvor, D., V. Dubreuil, J. Ronchail, M. Simões, and B. M. Funatsu (2014), Spatial patterns of rainfall regimes related to levels of double cropping agriculture systems in Mato Grosso (Brazil), *Int. J. Climatol.*, *34*(8), 2622–2633, doi:10.1002/joc.3863.

Aufdenkampe, A. K., E. Mayorga, P. A. Raymond, J. M. Melack, S. C. Doney, S. R. Alin, R. E. Aalto, and K. Yoo (2011), Riverine coupling of biogeochemical cycles between land, oceans, and atmosphere, *Front. Ecol. Environ.*, *9*(1), 53–60, doi:10.1890/100014.

Auguie, B. (2016), gridExtra: Miscellaneous functions for "grid" graphics. R package version 2.2.1. [Availabe at https://CRAN.R-project.org/package=gridExtra.]

Baldocchi, D., J. Tang, and L. Xu (2006), How switches and lags in biophysical regulators affect spatial-temporal variation of soil respiration in an oak-grass savanna, *J. Geophys. Res.*, *111*, G02008, doi:10.1029/2005JG000063.

Bass, A. M., D. O'Grady, M. Leblanc, S. Tweed, P. N. Nelson, and M. I. Bird (2014), Carbon dioxide and methane emissions from a wet-dry tropical floodplain in northern Australia, *Wetlands*, *34*(3), 619–627, doi:10.1007/s13157-014-0522-5.

Belger, L., B. R. Forsberg, and J. M. Melack (2011), Carbon dioxide and methane emissions from interfluvial wetlands in the upper Negro River basin, Brazil, *Biogeochemistry*, *105*(1–3), 171–183, doi:10.1007/s10533-010-9536-0.

Bivand, R. S., T. Keitt, and B. Rowlingson (2014), rgdal: Bindings for the geospatial data abstraction library, R package version 0.8–16. [Available at http://CRAN.R-project.org/package=rgal.]

Bivand, R. S., E. Pebesma, and V. Gomez-Rubio (2013), *Applied Spatial Data Analysis with R*, 2nd ed., Springer, New York.

Campbell, G. S., and J. M. Norman (1998), *An Introduction to Environmental Biophysics*, Springer, New York.

Carslaw, D. C., and K. Ropkins (2012), openair—An R package for air quality data analysis, *Environ. Modell. Softw.*, *27–28*, 52–61.

Carslaw, D. C., and K. Ropkins (2016), openair: Open-source tools for the analysis of air pollution data, R package version 1.8–6. [Available at http://CRAN.R-project.org/package=openair.]

Carvalho, P. V. (2013), Estudo de fluxo de CO_2 e do estoque de carbono do solo em área de interflúvio no Pantanal município de Poconé Mato Grosso, Universidade Federal de Mato Grosso, Cuiabá, Mato Grosso, Brazil. [Available at http://www.pgfa.ufmt.br/index.php/en/utilities/dissertations/264-paula-valeria-de-carvalho/file.]

Couto, E. G., and V. Oliveira (2011), The soil diversity of the Pantanal, in *The Pantanal: Ecology, Biodiversity and Sustainable Management of a Large Neotropical Seasonal Wetland*, edited by W. J. Junk et al., pp. 71–102, Pensoft Publ., Sofia, Bulgaria.

Couto, E. G., P. K. T. Jacomine, C. Nunes da Cunha, and A. B. Vecchiato (2002), *Guia da excursão técnica, paper presented at XIV Reunião Brasileira de Manejo e Conservação do Solo e da Água*, Universidade Federal de Mato Grosso, Cuiabá, MT, Brazil.

Couto, E. G., M. S. Johnson, O. B. Pinto Jr., and N. Leite (2012), Soil redox dynamics vary with landscape position and hydroperiod in the Pantanal wetland ecosystem, Abstract EP43A-0862 presented at 2012, Fall Meeting, AGU, San Francisco, Calif., 3–7 Dec.

Cueva, A., M. Bahn, M. Litvak, J. Pumpanen, and R. Vargas (2015), A multisite analysis of temporal random errors in soil CO_2 efflux, *J. Geophys. Res. Biogeosci*, *120*, 737–751, doi:10.1002/2014JG002690.

Dalmagro, H. J., M. S. Johnson, M. J. Lathuillière, O. B. Pinto Jr., and E. G. Couto (2013), Dissolved organic carbon quality assessed along the Cuiabá River of Mato Grosso, Brazil, using fluorescence spectroscopy, Abstract H41C-1235 presented at 2013, Fall Meeting, AGU, San Francisco, Calif., 9–13 Dec.

Dalmagro, H. J., M. J. Lathuillière, G. L. Vourlitis, R. C. Campos, O. B. Pinto Jr., M. S. Johnson, C. E. R. Ortiz, F. D. A. Lobo, and E. G. Couto (2016), Physiological responses to extreme hydrological events in the Pantanal wetland: Heterogeneity of a plant community containing super-dominant species, *J. Veg. Sci.*, *27*(3), 568–577, doi:10.1111/jvs.12379.

Dias, M. F. (2015), Dynamics of CO_2 efflux in two different ecosystems compositions, Dissertation, Department of Environmental Sciences, Univ. of Cuiabá, Cuiabá, Mato Grosso, Brazil.
Girard, P., I. Fantin-Cruz, S. M. Loverde de Oliveira, and S. K. Hamilton (2010), Small-scale spatial variation of inundation dynamics in a floodplain of the Pantanal (Brazil), *Hydrobiologia*, *638*(1), 223–233, doi:10.1007/s10750-009-0046-9.
Hamilton, S., S. Sippel, and J. Melack (1995), Oxygen depletion and carbon-dioxide and methane production in waters of the Pantanal wetland of Brazil, *Biogeochemistry*, *30*(2), 115–141, doi:10.1007/BF00002727.
Hashimoto, S., and J. Komatsu (2006), Relationships between soil CO_2 production, temperature, water content, and gas diffusivity: Implications for field studies through sensitivity analysis, *J. Fore. Res.*, *11*(1), 41–50, doi:10.1007/s10310-005-0185-4.
Hijmans, R. J. (2014), raster: Geographic data analysis and modeling, R package version 2.2–31. [Available at http://CRAN.R-project.org/package=raster.]
Huxman, T. E., et al. (2004), Precipitation pulses and carbon fluxes in semiarid and arid ecosystems, *Oecologia*, *141*, 254–268, doi:10.1007/s00442-004-1682-4.
Jarvis, P., et al. (2007), Drying and wetting of Mediterranean soils stimulates decomposition and carbon dioxide emission: The "birch" effect, *Tree Physiol.*, *27*, 929–940, doi:10.1093/treephys/27.7.929.
Jassal, R., T. Black, G. Drewitt, M. Novak, D. Gaumont-Guay, and Z. Nesic (2004), A model of the production and transport of CO_2 in soil: Predicting soil CO_2 concentrations and CO_2 efflux from a forest floor, *Agric. For. Meteorol.*, *124*(3–4), 219–236, doi:10.1016/j.agrformet.2004.01.013.
Jassal, R., A. Black, M. Novak, K. Morgenstern, Z. Nesic, and D. Gaumont-Guay (2005), Relationship between soil CO_2 concentrations and forest-floor CO_2 effluxes, *Agric. For. Meteorol.*, *130*(3–4), 176–192, doi:10.1016/j.agrformet.2005.03.005.
Jobbágy, E. G., and R. B. Jackson (2000), The vertical distribution of soil organic carbon and its relation to climate and vegetation, *Ecol. Appl.*, *10*(2), 423–436, doi:10.1890/1051-0761(2000)010[0423:TVDOSO]2.0.CO;2.
Johnson, M. S., M. F. Billet, K. J. Dinsmore, M. Wallin, K. E. Dyson, and R. S. Jassal (2009), Direct and continuous measurement of dissolved carbon dioxide in freshwater aquatic systems—Method and applications, *Ecohydrology*, *3*(1), 68–78, doi:10.1002/eco.95.
Johnson, M. S., E. G. Couto, O. B. Pinto Jr., J. Milesi, R. S. S. Amorim, I. A. M. Messias, and M. S. Biudes (2013), Soil CO_2 dynamics in a tree island soil of the Pantanal: The role of soil water potential, *PLoS One*, *8*(6), e64874, doi:10.1371/journal.pone.0064874.
Junk, W. J. (2013), Current state of knowledge regarding South America wetlands and their future under global climate change, *Aquat. Sci.*, *75*(1), 113–131, doi:10.1007/s00027-012-0253-8.
Junk, W. J., C. N. da Cunha, K. M. Wantzen, P. Petermann, C. Struessmann, M. I. Marques, and J. Adis (2006), Biodiversity and its conservation in the Pantanal of Mato Grosso, Brazil, *Aquat. Sci.*, *68*(3), 278–309, doi:10.1007/s00027-006-0851-4.
Junk, W. J., S. An, C. M. Finlayson, B. Gopal, J. Kvet, S. A. Mitchell, W. J. Mitsch, and R. D. Robarts (2013), Current state of knowledge regarding the world's wetlands and their future under global climate change: A synthesis, *Aquat. Sci.*, *75*(1), 151–167, doi:10.1007/s00027-012-0278-z.
Junk, W. J., et al. (2014), Brazilian wetlands: Their definition, delineation, and classification for research, sustainable management, and protection, *Aquat. Conserv. Mar. Freshwater Ecosyst.*, *24*(1), 5–22, doi:10.1002/aqc.2386.
Kim, D., R. Vargas, B. Bond-Lamberty, and M. R. Turetsky (2012), Effects of soil rewetting and thawing on soil gas fluxes: A review of current literature and suggestions for future research, *Biogeosciences*, *9*(7), 2459–2483, doi:10.5194/bg-9-2459-2012.
Lee, X., H. J. Wu, J. Sigler, C. Oishi, and T. Siccama (2004), Rapid and transient response of soil respiration to rain, *Global Change Biol.*, *10*, 1017–1026, doi:10.1111/j.1365-2486.2004.00787.x.
Liebmann, B., S. J. Camargo, A. Seth, J. A. Marengo, L. M. V. Carvalho, D. Allured, R. Fu, and C. S. Vera (2007), Onset and end of the rainy season in South America in observations and the ECHAM 4.5 atmospheric general circulation model, *J. Clim.*, *20*, 2037–2050, doi:10.1175/JCLI4122.1.
Loarie, S. R., D. B. Lobell, G. P. Asner, Q. Mu, and C. B. Field (2011), Direct impacts on local climate of sugar cane expansion in Brazil, *Nat. Clim. Change*, *1*, 105–109, doi:10.1038/nclimate1067.
Marañón-Jiménez, S., J. Castro, A. S. Kowalski, P. Serrano-Ortiz, B. R. Reverter, E. P. Sanchez-Cañete, and R. Zamora (2011), Post-fire soil respiration in relation to burnt wood management in a Mediterranean mountain ecosystem, *For. Ecol. Manage.*, *261*, 1436–1447, doi:10.1016/j.foreco.2011.01.030.
Marshall, T. J. (1959), Gas diffusion in porous media, *Science*, *130*, 100–102, doi:10.1126/science.130.3367.100-a.
Messias, I. A. M., E. G. Couto, O. B. Pinto-Jr, and M. S. Johnson (2013), Monitoramento contínuo do potencial redox e de variáveis complementares em ambiente hipersazonal no Pantanal norte, *Rev. Bras. Ciênc. Solo*, *37*, 632–639.
Millington, R. J., and J. P. Quirk (1961), Permeability of porous solids, *Trans. Faraday Soc.*, *57*, 1–8, doi:10.1039/TF9615701200.
Millenium Ecosystem Assessment (2005), *Ecosystems and Human Wellbeing: Wetlands and Water*, World Resources Institute, Washington, D. C.
Mitra, S., R. Wassmann, and P. Vlek (2005), An appraisal of global wetland area and its organic carbon stock, *Curr. Sci.*, *88*(1), 25–35.
Mitsch, W. J., and J. G. Gosselink (2015), in *Wetlands*, edited by W. J. Mitsch and J. G. Gosselink, John Wiley, N. J.
Mitsch, W. J., A. Nahlik, P. Wolski, B. Bernal, L. Zhang, and L. Ramberg (2010), Tropical wetlands: Seasonal hydrologic pulsing, carbon sequestration, and methane emissions, *Wetlands Ecol. Manage.*, *18*(5), 573–586, doi:10.1007/s11273-009-9164-4.
Moldrup, P., T. Olson, T. Yamagushi, P. Schjonning, and D. E. Rolston (1999), Modeling diffusion and reaction in soil. IX. The Buckingham-Burdine-Campbell equation for gas diffusivity in undisturbed soil, *Soil Sci.*, *164*, 542–551.
Mu, Q., M. Zhao, and S. W. Running (2011), Improvements to a MODIS global terrestrial evapotranspiration algorithm, *Remote Sens. Environ.*, *115*, 1781–1800, doi:10.1016/j.rse.2011.02.019.
Mualem, Y. (1976), A new model for predicting the hydraulic conductivity of unsaturated porous media, *Water Resour. Res.*, *12*, 513–522.
Nascimento, A. F., S. A. C. Furquim, R. C. Graham, R. M. Beirigo, J. C. Oliveira Jr., E. G. Couto, and P. Vidal-Torrado (2015), Pedogenesis in a Pleistocene fluvial system of the Northern Pantanal-Brazil, *Geoderma*, *255–256*, 58–72, doi:10.1016/j.geoderma.2015.04.025.
Neue, H. U., J. L. Gaunt, Z. P. Wang, P. Becker-Heidmann, and C. Quijano (1997), Carbon in tropical wetlands, *Geoderma*, *79*, 163–185, doi:10.1016/S0016-7061(97)00041-4.
Pebesma, E., and R. S. Bivand (2005), Classes and methods for spatial data in R, R News 5(2). [Available at http://cran.r-project.org/doc/Rnews/.]
Penman, H. L. (1940), Gas and vapour movement in the soil. I. The diffusion of vapours through porous solids. II. The diffusion of carbon dioxide through porous solids, *J. Agric. Sci.*, *30*(437–462), 570–581.
Pezeshki, S. R., and R. D. Delaune (2012), Soil oxidation-reduction in wetlands and its impact on plant functioning, *Biology*, *1*, 196–221, doi:10.3390/biology1020196.
R Core Team (2016), *R: A Language and Environment for Statistical Computing*, R Foundation for Statistical Computing, Vienna, Austria.
Richardson, A. D., et al. (2006), A multi-site analysis of random error in tower-based measurements of carbon and energy fluxes, *Agric. For. Meteorol.*, *136*, 1–18, doi:10.1016/j.agrformet.2006.01.007.
Schindler, U., W. Durner, G. von Unold, L. Mueller, and R. Wieland (2010), The evaporation method: Extending the measurement range of soil hydraulic properties using the air-entry pressure of the ceramic cup, *J. Plant Nutr. Soil Sci.*, *173*(4), 563–572, doi:10.1002/jpln.200900201.

Tang, J., D. Baldocchi, Y. Qi, and L. Xu (2003), Assessing soil CO_2 efflux using continuous measurements of CO_2 profiles in soils with small solid-state sensors, *Agric. For. Meteorol.*, *118*(3–4), 207–220, doi:10.1016/S0168-1923(03)00112-6.

Therneau, T., T. Lumley, K. Halvorsen, K. Hornik (2014), date: Functions for handling dates, R package version 1.2–34.

Vaisala (2017), *GMM220 Series CO_2 Transmitter Modules, M01011EN-D*, Vaisala Inc., Helsinki, Finland.

Van Genuchten, M. (1980), A closed-form equation for predicting the hydraulic conductivity of unsaturated soils, *Soil Sci. Soc. Am. J.*, *44*(5), 892–898.

Vargas, R., et al. (2010), Looking deeper into the soil: Biophysical controls and seasonal lags of soil CO_2 production and efflux, *Ecol. Appl.*, *20*(6), 1569–1582, doi:10.1890/09-0693.1.

Vepraskas, M. J., and A. P. Faulkner (2000), Redox chemistry of hydric soils, in *Wetland Soils: Genesis Hydrology, Landscapes and Classification*, edited by M. J. Vepraskas, C. B. Craft, and J. L. Richardson, pp. 85–105, CRC Press LLC, Boca Raton, Fla.

Vourlitis, G. L., F. D. A. Lobo, S. Lawrence, K. Holt, A. Zappia, O. B. Pinto Jr., and J. D. S. Nogueira (2014), Nutrient resorption in tropical savanna forests and woodlands of central Brazil, *Plant Ecol.*, *215*, 963–975, doi:10.1007/s11258-014-0348-5.

Vourlitis, G. L., F. D. A. Lobo, O. B. Pinto Jr., A. Zappia, H. J. Dalmagro, P. H. Zanella de Arruda, and J. D. S. Nogueira (2015), Variations in aboveground vegetation structure along a nutrient availability gradient in the Brazilian Pantanal, *Plant Soil*, *389*(1–2), 307–321, doi:10.1007/s11104-014-2364-6.

Wickham, H. (2009), *ggplot2: Elegant Graphics for Data Analysis*, Springer-Verlag, New York.

Wickham, H. (2016), scales: Scale functions for visualization. R package version 0.4.0. [Available at https://CRAN.R-project.org/package=scales.]